

Article

Aptamer Targets Triple-Negative Breast Cancer through Specific Binding to Surface CD49c

Quanyuan Wan ¹, Zihua Zeng ¹, Jianjun Qi ¹, Yingxin Zhao ², Xiaohui Liu ¹, Zhenghu Chen ¹ , Haijun Zhou ¹ and Youli Zu ^{1,*}

¹ Department of Pathology and Genomic Medicine, Houston Methodist Hospital, Houston, TX 77030, USA; qyuanwan@gmail.com (Q.W.); zzeng@houstonmethodist.org (Z.Z.); jqj@houstonmethodist.org (J.Q.); lcswyh@126.com (X.L.); zchen2@houstonmethodist.org (Z.C.); hzhou@houstonmethodist.org (H.Z.)

² Department of Internal Medicine, University of Texas Medical Branch, Galveston, TX 77555, USA; yizhao@utmb.edu

* Correspondence: yzu@houstonmethodist.org

Simple Summary: Targeted therapy directed against many biomarkers has not shown significant improvement in outcome in TNBC, and therefore it is urgent to discover more biomarker candidates. Here, we found a DNA aptamer that bound to TNBC cells and identified CD49c as a specific surface marker for TNBC cells using the aptamer-facilitated biomarker discovery technology. The findings suggest that this DNA aptamer can be a drug delivery vehicle and CD49c is a potential target of targeted therapy for TNBC.

Abstract: Although targeted cancer therapy can induce higher therapeutic efficacy and cause fewer side effects in patients, the lack of targetable biomarkers on triple-negative breast cancer (TNBC) cells limits the development of targeted therapies by antibody technology. Therefore, we investigated an alternative approach to target TNBC by using the PDGC21T aptamer, which selectively binds to poorly differentiated carcinoma cells and tumor tissues, although the cellular target is still unknown. We found that synthetic aptamer probes specifically bound cultured TNBC cells in vitro and selectively targeted TNBC xenografts in vivo. Subsequently, to identify the target molecule on TNBC cells, we performed aptamer-mediated immunoprecipitation in lysed cell membranes followed by liquid chromatography tandem mass spectrometry (LC-MS/MS). Sequencing analysis revealed a highly conserved peptide sequence consistent with the cell surface protein CD49c (integrin $\alpha 3$). For target validation, we stained cultured TNBC and non-TNBC cells with an aptamer probe or a CD49c antibody and found similar cell staining patterns. Finally, competition cell-binding assays using both aptamer and anti-CD49c antibody revealed that CD49c is the biomarker targeted by the PDGC21T aptamer on TNBC cells. Our findings provide a molecular foundation for the development of targeted TNBC therapy using the PDGC21T aptamer as a targeting ligand.

Keywords: aptamer ligand; biomarker identification; integrin $\alpha 3$ /CD49c; triple-negative breast cancer (TNBC); targeted cancer therapy



Citation: Wan, Q.; Zeng, Z.; Qi, J.; Zhao, Y.; Liu, X.; Chen, Z.; Zhou, H.; Zu, Y. Aptamer Targets Triple-Negative Breast Cancer through Specific Binding to Surface CD49c. *Cancers* **2022**, *14*, 1570. <https://doi.org/10.3390/cancers14061570>

Academic Editors: Maurizio Di Bonito, Michelino De Laurentiis and Monica Cantile

Received: 27 January 2022

Accepted: 14 March 2022

Published: 18 March 2022

Publisher's Note: MDPI stays neutral with regard to jurisdictional claims in published maps and institutional affiliations.



Copyright: © 2022 by the authors. Licensee MDPI, Basel, Switzerland. This article is an open access article distributed under the terms and conditions of the Creative Commons Attribution (CC BY) license (<https://creativecommons.org/licenses/by/4.0/>).

1. Introduction

Breast cancer is the most common cancer among women worldwide, and is the fifth leading cause of cancer mortality, with an estimated 2.3 million new cases representing 11.7% of all cancer cases in 2020 [1]. Breast cancers are categorized into six subtypes based on the expression of cell surface molecular markers. For therapeutic purposes, breast cancers are categorized into three subtypes: estrogen and progesterone receptor (ER, PR)-positive, human epidermal growth factor receptor 2 (HER2)-positive, and triple (ER, PR, and HER2)-negative [2]. The triple-negative breast cancer (TNBC) subtype accounts for 15–20% of all breast cancers. Clinically, TNBC grows and spreads faster than other breast cancer subtypes

and therefore tends to be more aggressive, with a higher potential for disease metastasis and recurrence. Pathologically, TNBC tumor cells are poorly differentiated and do not express ER, PR, or HER2. Therefore, TNBC does not respond to ER/PR-based hormonal therapy or HER2-targeting therapies, which are used clinically to treat other types of breast cancers. The lack of specific biomarkers on TNBC cells impedes the development of targeted therapeutic approaches. Currently, a combination of surgery and chemotherapy is the standard of care to treat TNBC. However, none of these are specific for TNBC, and chemotherapy may have severe off-target toxicity in normal tissues [2,3].

Nucleic acid aptamers are small-molecule ligands comprising short, single-strand DNA (ssDNA) or ssRNA. Target-specific aptamers can be developed from ssRNA/ssDNA libraries via a defined experimental process called the systematic evolution of ligands by exponential enrichment (SELEX). Aptamers can be developed via the SELEX approach by using cells as the targets, namely cell-based SELEX (cSELEX). Importantly, the cSELEX allows researchers to develop aptamers specific for cells of interest without knowledge of target molecules on cell surface or no known targetable biomarkers available [4–6]. Such aptamers developed by cSELEX have been studied for *in vivo* tumor imaging, including B-cell lymphoma [7], colorectal cancer [8], and lung cancer [9]. In addition, the aptamers can function as a vehicle for targeted delivery of miRNA/siRNA or anticarcinogens [10], and act as an anti-cancer agent [11,12]. Moreover, the aptamers developed by the cSELEX approach are valuable tools to identify new specific biomarkers on cells of interest via the aptamer-facilitated biomarker discovery (AptaBiD) technology [13]. A recent study using the cSELEX approach identified the ssDNA aptamer (PDGC21T), which recognizes and selectively binds to poorly differentiated gastric cancer tissue in patient specimens, even though the identity of the target molecule(s) was unknown [14]. Because TNBC is also poorly differentiated, we explored whether the aptamer could target TNBC cells. Both *in vitro* and *in vivo* studies demonstrated that the synthetic PDGC21T aptamer could bind TNBC cells with high affinity and target TNBC cell-xenograft tumors. To identify the target of the PDGC21T aptamer, we conducted an aptamer-mediated co-precipitation study and subsequent mass spectrometry-based proteomics assays. Peptide identification analysis revealed that the target of PDGC21T is CD49c (integrin alpha 3) on TNBC cells. These findings provide a foundation for the development of an aptamer-guided approach for imaging detection and targeted therapy in TNBC tumors.

2. Materials and Methods

2.1. Cell Culture

The TNBC cell lines were kind gifts from Dr. Jenny C. Chang's lab at the Houston Methodist Academic Institute. The other cells were purchased from American Type Culture Collection (ATCC, Manassas, VA, USA), cultured, and stored in our laboratory. Cell lines were cultured in Roswell Park Memorial Institute (RPMI)-1640 medium (Corning, Corning, NY, USA) supplemented with 10% FBS (Corning), 100 units/mL penicillin (Gibco, Waltham, MA, USA), and 100 µg/mL streptomycin (Gibco). For cell passage, 0.25% trypsin with ethylenediaminetetraacetic acid (Corning) and non-enzymatic cell dissociation solution (Corning) were used. All cells were grown at 37 °C in 95% air/5% CO₂. All experiments were performed with mycoplasma-free cells as tested with e-Myco™ plus mycoplasma PCR detection kit (iNtRON Biotechnology, Seoul, South Korea).

2.2. Aptamer Binding Assay

All aptamers, including 5'-dye-labeled or 5'-biotinylated aptamers, were purchased from Integrated DNA Technologies (IDT Inc., Coralville, IA, USA). Dry DNA oligos were dissolved to a storage concentration of 100 µM with PM buffer (1 × PBS (Corning) supplemented with 5 mM MgCl₂ (Sigma-Aldrich, St. Louis, MO, USA)) and stored at −20 °C until further use. Before use, aptamers were thawed and diluted to 10 µM with PM buffer, heated to 95 °C, and immediately cooled in ice for at least 10 min. Before cell-binding assays, the biotinylated aptamer used for the binding test was incubated with streptavidin-conjugated

Cy3 (Invitrogen, Carlsbad, CA, USA) at 37 °C for 30 min to link the aptamer with the Cy3 dye.

Cells were harvested using non-enzymatic cell dissociation solution and then washed once with PBS. Then, cells were distributed into Falcon[®] 5 mL round-bottomed polystyrene test tubes (Corning) and incubated with varying concentrations of dye-labeled aptamers, random ssDNA sequences, antibodies, or IgG control in 100 µL of binding buffer (1 × PBS supplemented with 0.1 g/L yeast tRNA (Invitrogen, Waltham, MA, USA), 4.5 g/L glucose (Gibco), 1.0 g/L bovine serum albumin (Thermo Scientific, Waltham, MA, USA), and 5 mM MgCl₂ (Sigma-Aldrich)). After incubation at room temperature (RT) for 15–30 min, cells were collected by means of centrifugation at 400 × g for 5 min. Then, cells were resuspended with 1 mL of washing buffer (1 × PBS supplemented with 4.5 g/L glucose and 5 mM MgCl₂) and washed once. Subsequently, cells were collected by means of centrifugation and re-suspended in flow cytometer running buffer (1 × PBS supplemented with 2% FBS and 5 mM MgCl₂). Flow cytometry was then performed using a BD LSR II Flow Cytometer (BD Biosciences, San Jose, CA, USA) to measure the fluorescence signal from cell-bound aptamers or antibodies. The fluorescence was observed through fluorescent microscopic imaging (Olympus IX81, Olympus America, Melville, NY, USA). Flow cytometry data were analyzed using FlowJo software (version: X 10.0.7r2, FlowJo, Ashland, OR, USA).

2.3. Aptamer-Antibody Competition Binding Assay

To determine whether PDGC21T affects anti-CD49c binding, a final concentration of 1 µM Cy3-labeled PDGC21T or a random ssDNA library (negative control) was pre-incubated with MDA-MB-231 or HCC38 cells at RT for 15 min. Then, 1 µL of PE-labeled anti-CD49c (Clone C3 II.1, BD Pharmingen[™], San Diego, CA, USA) was added to cells and incubation continued for 15 min. As controls, PE-labeled anti-CD49c or IgG isotype (κ Isotype control, Clone MOPC-21, BD Pharmingen[™]) were incubated with MDA-MB-231 or HCC38 cells at RT for 15 min. To determine whether anti-CD49c affects PDGC21T binding, 5 µL of PE-labeled anti-CD49c or IgG isotype were pre-incubated with MDA-MB-231 or HCC38 cells at RT for 15 min. Then, fluorescein amidite (FAM)-labeled PDGC21T was added to cells at a final concentration of 200 nM and incubation continued for 15 min. As a blank control, FAM-labeled PDGC21T or a random library was incubated with MDA-MB-231 or HCC38 cells at RT for 15 min. After incubation, cells were washed once with wash buffer and re-suspended in running buffer for flow cytometry.

2.4. PDGC21T Pull-Down Assay

Aptamer-based pull-down and high-performance liquid chromatography mass spectrum (HPLC-MS) were used to identify PDGC21T targets. The pull-down assay was performed according to a previously published procedure using a biotinylated aptamer [15]. To measure the binding ability of the biotinylated PDGC21T, two approaches were used. One approach is to link the biotinylated PDGC21T with the streptavidin-Cy3, as described previously. Another approach is to perform the competitive assay. Briefly, a final concentration of 1 µM biotinylated PDGC21T was pre-incubated with MDA-MB-231 cells at RT for 15 min. Then, Cy3-labeled PDGC21T was added to cells at a final concentration of 200 nM and incubation continued for 15 min. Binding ability was measured using flow cytometry. Pull-down was performed after confirming the binding ability of the biotinylated PDGC21T.

Ten million cells were harvested using trypsin and washed once with PBS. After washing, cells were re-suspended and lysed in 1.8 mL of 50 mM Tris-Cl buffer (pH 7.4) (Sigma-Aldrich) supplemented with phenylmethylsulfonyl fluoride (PMSF) (Sigma-Aldrich) and proteinase inhibitor cocktail (Sigma-Aldrich) for 30 min at 4 °C. After incubation, cell debris was collected by means of centrifugation at 12,000 × g for 3 min at 4 °C and washed three times with 50 mM Tris-Cl buffer (pH 7.4) supplemented with PMSF. The pellet was resuspended and further lysed with 600 µL of lysis buffer (1 × PBS, supplemented with 5 mM MgCl₂, 1% Triton X-100 (Sigma-Aldrich), PMSF, and proteinase inhibitor cocktail)

for 30 min at 4 °C. After lysing, the supernatant was collected by means of centrifugation at 12,000× *g* for 5 min at 4 °C. The supernatant was aliquoted into three clean 2 mL tubes and pre-heated biotin-labeled PDGC21T aptamer or a random ssDNA library was added (final aptamer concentration, 2 μM). Rotated incubation was performed at 4 °C overnight. The next day, pre-washed streptavidin-sepharose (GE Healthcare, Marlborough, MA, USA) (200 μL of original volume/tube) was added and tubes were incubated with rotation for 1 h at 4 °C. After incubation, agarose beads were collected and washed three times with lysis buffer by centrifugation at 12,000× *g* for 5 min at 4 °C. Finally, 10 μL of 5× SDS sample loading buffer was added into each tube containing the collected agarose beads, and samples were heated at 85 °C for 10 min. Supernatant was collected by centrifugation at 12,000× *g* for 5 min at RT. A 15 μL aliquot of supernatant was loaded into the corresponding wells of a 4–15% Mini-PROTEAN® TGX™ precast protein gel (Bio-Rad, Hercules, CA, USA) and electrophoresed at 90 V for 2 h. The silver stain procedure for the gel was conducted according to the manufacturer's instructions (Pierce™ Silver Stain kit; Thermo Scientific). Protein bands of interest were excised for further liquid chromatography tandem mass spectrometry (LC-MS/MS) analysis (Supplemental Materials and Methods) [16–19].

2.5. PDGC21T PEGylation

PDGC21T PEGylation was performed as described previously with minor modifications [20]. Briefly, 120 μg of ^{IRD800CW}PDGC21T was dissolved in 800 μL of 0.1 M NaHCO₃/CH₃CN (*v/v* = 1:1, pH 9.0) (Sigma-Aldrich), and 20 mg of mPEG-NHS (Nanocs, New York, NY, USA) was added to this solution. The mixture was incubated overnight at RT with gentle shaking. The reaction was monitored by reversed-phase HPLC (RP-HPLC) using a PRP-1 analytic column (4.1 mm × 150 mm, 10 μm, HAMILTON Corporation, Reno, NV, USA) at a flow rate of 1 mL/min. A 15 min linear gradient from 0% solvent A [100 mM triethylammonium acetate (Sigma-Aldrich) in water, pH 7] to 100% solvent B [5% solvent A in CH₃CN (Sigma-Aldrich)] was used for each HPLC run. The resulting ^{IRD800CW}PDGC21T_{PEG5000} was purified using a PRP-1 semi-preparative column (10 mm × 250 mm, 10 μm, HAMILTON Corporation) at a flow rate of 3 mL/min. An 18 min linear gradient from 0% solvent A (100 mM triethylammonium acetate in water, pH 7) to 85% solvent B was used for each HPLC run. The fractions of ^{IRD800CW}PDGC21T_{PEG5000} were collected and solvents were removed with SpeedVac concentrator (SPD131DDA, Thermo Scientific). The purified ^{IRD800CW}PDGC21T_{PEG5000} was confirmed with a sodium dodecyl sulphate-polyacrylamide gel electrophoresis (SDS-PAGE) assay.

2.6. Tumor Xenograft and In Vivo and Ex Vivo PDGC21T Targeting

For PDGC21T targeting, NOD.Cg-Prkdc^{scid} Il2rg^{tm1Wjl}/SzJ (NSG) mice from the Jackson Laboratory were subcutaneously injected with 3 × 10⁶ of either HCC1937, SUM159PT, MDA-MB-231, HCC38, Hs578T, or MCF7 breast cancer cells in the lower back. Tumor size was measured using a vernier caliper and tumor volume was calculated using the following formula:

$$\text{tumor volume} = \text{tumor length} \times \text{tumor width}^2 \times 0.52 \quad (1)$$

Two months after tumor inoculation or when tumor volume reached 0.5 cm³, tumor-bearing mice were injected intravenously with a 0.067 nmol/dose (1.33 μg/dose) of ^{IRD800CW}PDGC21T or ^{IRD800CW}PDGC21T_{PEG5000}. Before injection, aptamers were heated at 95 °C for 5 min followed by an ice bath for at least 10 min. In vivo imaging was performed using an in vivo imaging system (Xenogen IVIS-200, Caliper Life Sciences, Hopkinton, MA, USA) at 30 min, 4 h, and 24 h post-aptamer injection. IRDye800CW-conjugated aptamers were observed under fluorescent settings at excitation and emission wavelengths of 745 and 820 nm, respectively. After in vivo imaging at 24 h post-aptamer injection, mice were euthanized. The heart, lung, kidney, liver, spleen, and tumor were removed and imaged. All images were analyzed using Living Image Software (version 4.7.4, Caliper Life Sciences, Waltham, MA, USA).

3.2. PDGC21T Aptamer Targets Xenograft TNBC Tumors

In an *in vivo* targeting study, mouse models with xenograft tumors derived from TNBC cells were developed. Aptamers were labeled with the near-infrared dye IRD800CW at the 5'-end to formulate IRD800CW PDGC21T. Because the polyethylene glycol (PEG) modification can increase the stability and prolong the blood circulation half-life of oligonucleotides [21], IRD800CW PDGC21T aptamers were conjugated with 5 kDa PEG at the 3'-end (Figure 2A), and resultant IRD800CW PDGC21T_{PEG5000} aptamers were purified using RP-HPLC (Figures S1 and S2). IRD800CW PDGC21T_{PEG5000} aptamer cell binding was initially tested *in vitro* as earlier described. Flow cytometry analysis revealed that IRD800CW PDGC21T_{PEG5000} aptamers bound TNBC cells (MDA-MB-231 and HCC38) but did not react with MCF7 cells (Figure 2B).

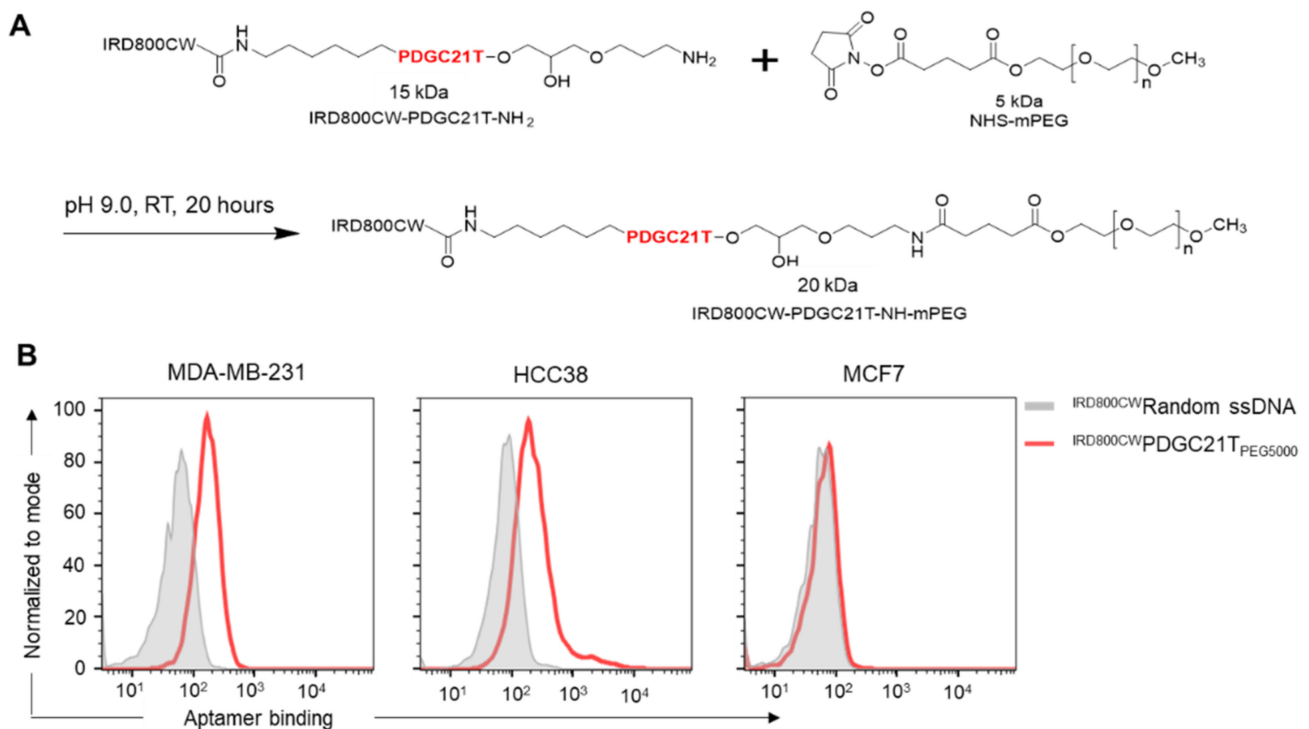


Figure 2. Preparation and validation of IRD800CW PDGC21T_{PEG5000} aptamers. (A) Schematic showing IRD800CW PDGC21T_{PEG5000} aptamer production. (B) Flow cytometry analysis of IRD800CW PDGC21T_{PEG5000} aptamer binding to TNBC cells. The final incubation concentration of aptamer or random ssDNA was 200 nM.

In an *in vivo* targeting study, mouse models of TNBC were developed using HCC1937, HCC38, MDA-MB-231, SUM159PT, and Hs578T xenograft tumors. In a control group, xenograft tumors derived from non-TNBC cells (MCF7) were used. Once xenograft tumors reached ≥ 0.5 cm³, IRD800CW PDGC21T_{PEG5000} aptamers were administered via the tail vein (Figure 3A). In an *in vivo* biostability study, IRD800CW PDGC21T aptamers were analyzed. Mice underwent optical imaging scans at 30 min, 4 h, and 24 h post-aptamer administration. Both aptamer probes specifically targeted MDA-MB-231 tumors with detectable imaging signals (Figure 3B). Notably, relative to IRD800CW PDGC21T aptamers, IRD800CW PDGC21T_{PEG5000} aptamers showed superior enhancement in MDA-MB-231 tumors and imaging signals lasted longer, up to 24 h post-aptamer administration. Specific TNBC tumor targeting by IRD800CW PDGC21T_{PEG5000} aptamers was also confirmed in mice bearing xenograft tumors derived from HCC1937, HCC38, SUM159PT, or Hs578T cells (Figure S3A–C). To rule out non-specific imaging, IRD800CW PDGC21T_{PEG5000} aptamers were administered to mice with non-TNBC xenograft tumors derived from MCF7 cells, and a whole-body imaging scan was performed as earlier described. Though weak signals were

detected peripherally in MCF7 tumor sides at 30 min post-aptamer administration, they faded rapidly and became undetectable (Figure 3C).

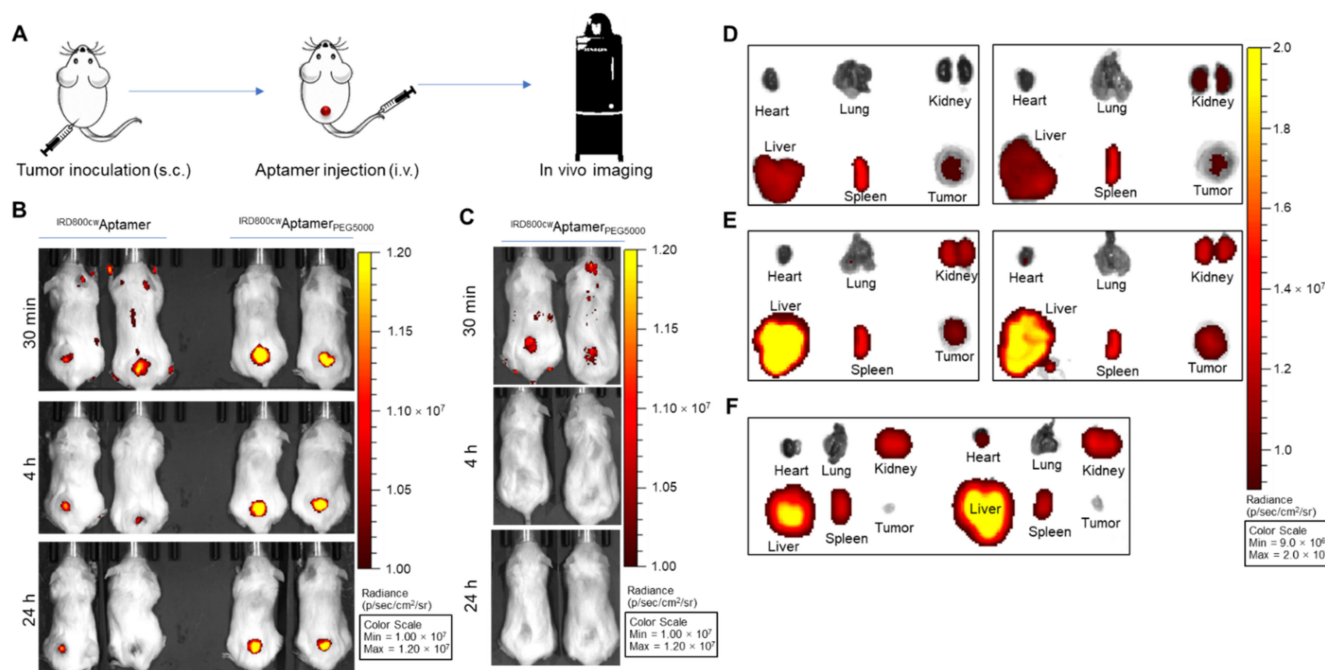


Figure 3. The $^{IRD800CW}PDGC21T_{PEG5000}$ aptamer specifically targets TNBC xenograft tumors and has an extended in vivo half-life. (A) Flow diagram of the in vivo tumor targeting study using aptamer probes. The red sphere indicates the xenograft tumor site. s.c., subcutaneous; i.v., intravenous. (B) Relative to $^{IRD800CW}PDGC21T$ aptamers, the signal enhancement from $^{IRD800CW}PDGC21T_{PEG5000}$ aptamers was stronger and persisted longer in MDA-MB-231 tumors (up to 24 h post-aptamer administration). (C) In contrast, weak signals were observed peripherally in MCF7 tumor sites at 30 min post $^{IRD800CW}PDGC21T_{PEG5000}$ aptamer administration but faded rapidly and became undetectable under the same imaging conditions. (D,E) Ex vivo imaging of resected MDA-MB-231 xenograft tumors, hearts, lungs, kidneys, livers, and spleens from mice treated with $^{IRD800CW}PDGC21T$ aptamers (D), or $^{IRD800CW}PDGC21T_{PEG5000}$ aptamers (E) post-whole-body imaging. (F) Ex vivo imaging of resected MCF7 xenograft tumors and major organs from mice treated with the $^{IRD800CW}PDGC21T_{PEG5000}$ aptamers.

To confirm the in vivo imaging results, xenograft tumors and major organs were collected after whole-body imaging. Ex vivo imaging demonstrated that mice treated with $^{IRD800CW}PDGC21T_{PEG5000}$ aptamers showed stronger signal enhancement in TNBC tumors relative to those treated with $^{IRD800CW}PDGC21T$ aptamers (Figure 3D,E, and Figure S3D–F). In contrast, no signals were detected in non-TNBC tumors in mice treated with $^{IRD800CW}PDGC21T_{PEG5000}$ aptamers (Figure 3F), though a similar pattern of the background signal was present. Taken together, these findings indicate that PDGC21T aptamers selectively target TNBC xenograft tumors and PEGylation significantly improves the circulation half-life of PDGC21T aptamers.

3.3. PDGC21T Targets Human CD49c

Because the PDGC21T aptamer can selectively bind intact TNBC cells and xenograft tumors, its target is considered a cell surface molecule or membrane protein. To discover the identity of the PDGC21T aptamer target on tumor cells, biotinylated PDGC21T was synthesized. First, the cell-binding capacity of the biotinylated aptamer was confirmed in MDA-MB-231 cells using a Cy3-labeled aptamer probe as a control (Figure 4A). Subsequently, the membrane protein fraction derived from TNBC cells (MDA-MB-231, HCC38, and Hs578T mixtures) was prepared, and target co-precipitation by biotinylated aptamer

was performed. As a background control, biotinylated ssDNA containing a random sequence of the same length as the PDGC21T aptamer was used. The resultant co-precipitated complexes were pulled down with streptavidin-conjugated agarose beads, separated by SDS-PAGE, and developed with silver staining. A protein band with a relative molecular weight of ~118 kDa was detected in a co-precipitated complex of PDGC21T aptamer, but not the random ssDNA control or blank sample (Figures 4B and S4). The same set of co-precipitation assays were carried out using membrane fractions of non-TNBC cells (mixture of MCF7, T47D, and Jurkat cells), and this protein band was not detected in samples incubated with PDGC21T aptamer or the random ssDNA control (Figure 4B).

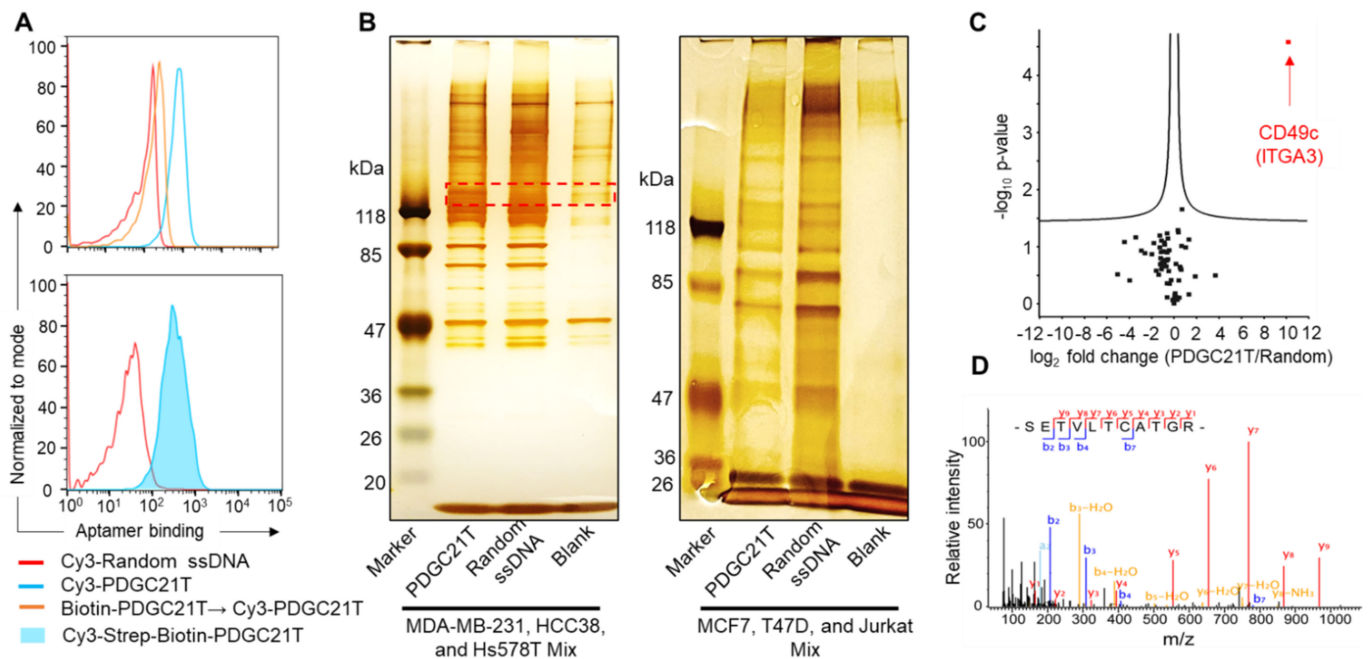


Figure 4. Identification of the PDGC21T aptamer target molecule. (A) Biotinylated PDGC21T aptamer targeted MDA-MB-231 cells with a similar binding capacity to that of Cy3-labeled PDGC21T aptamers. In contrast, random ssDNA controls did not bind MDA-MB-231 cells. Biotin-PDGC21T → Cy3-PDGC21T indicates MDA-MB-231 cells that were first incubated with biotinylated PDGC21T and then incubated with Cy3-labeled PDGC21T. The final incubation concentration of aptamers or random ssDNA was 200 nM. (B) Aptamer-mediated immunoprecipitation assays. Membrane proteins derived from TNBC cells (MDA-MB-231, HCC38, and Hs578T mixtures) and non-TNBC cells (MCF7, T47D, and Jurkat mixture) were prepared and used for co-precipitation with biotinylated PDGC21T aptamer, biotinylated random ssDNA, or vehicle alone as a blank control. Resultant aptamer and target complexes were pulled down by streptavidin-immobilized agarose beads and separated on sodium dodecyl sulphate-polyacrylamide gel electrophoresis (SDS-PAGE), followed by silver staining. The red-dotted box shows the protein band of interest, which was collected for liquid chromatography tandem mass spectrometry (LC-MS/MS) identity analysis. The uncropped figures are shown in Figure S4. (C,D) LC-MS/MS identification of the target of PDGC21T. The proteins detected in PDGC21T aptamer and random sequence pull-down experiments were identified and quantified with label-free LC-MS. (C) Volcano plot of identified proteins. Each dot represents one protein. Proteins above the cutoff curves are statistically significant (Student's *t*-test with 1% permutation-based FDR below 0.01). (D) Annotated MS/MS spectra of CD49c (ITGA3) peptide, STEVLTCATGR.

The protein band was collected for label-free LC-MS/MS analysis. A total of 64 proteins with <1% false-positive rate (FDR) were detected and quantified (Tables S1 and S2). Student's *t*-test with permutation-based FDR correction was used to identify proteins whose abundance varied significantly between the two samples (PDGC21T aptamer vs. random ssDNA). Integrin $\alpha 3$ (CD49c, encoded by *ITGA3*) was the only protein significantly (fold

change = 1143, $p = 1.3 \times 10^{-18}$) enriched in the PDGC21T aptamer co-precipitation complex, indicating a specific interaction between the PDGC21T aptamer and CD49c (Figure 4C). Six unique CD49c peptides were identified in this experiment. The annotated MS/MS spectra of one of the identified CD49c peptides with the sequence STEVLTCATGR are shown in Figure 4D.

To confirm that PDGC21T aptamer targeted TNBC cells through cell surface CD49c, a CD49c antibody (anti-CD49c) was used as a cell-binding control. Ten TNBC and eight non-TNBC cell lines were treated with the PDGC21T aptamer or anti-CD49c under identical conditions, and resultant cell staining patterns were compared. Flow cytometry analysis revealed that PDGC21T selectively targeted TNBC cells with high binding affinity. A nearly identical staining pattern to that obtained with anti-CD49c was observed (Figure 5A). In contrast, both the aptamer and antibody had little/no binding to non-TNBC cells, which express almost no CD49c (Figure 5B). The resultant mean fluorescent intensity of cell binding was quantified and graphed for the comparison of both the aptamer and antibody (Figure 5C,D, and Table S3).

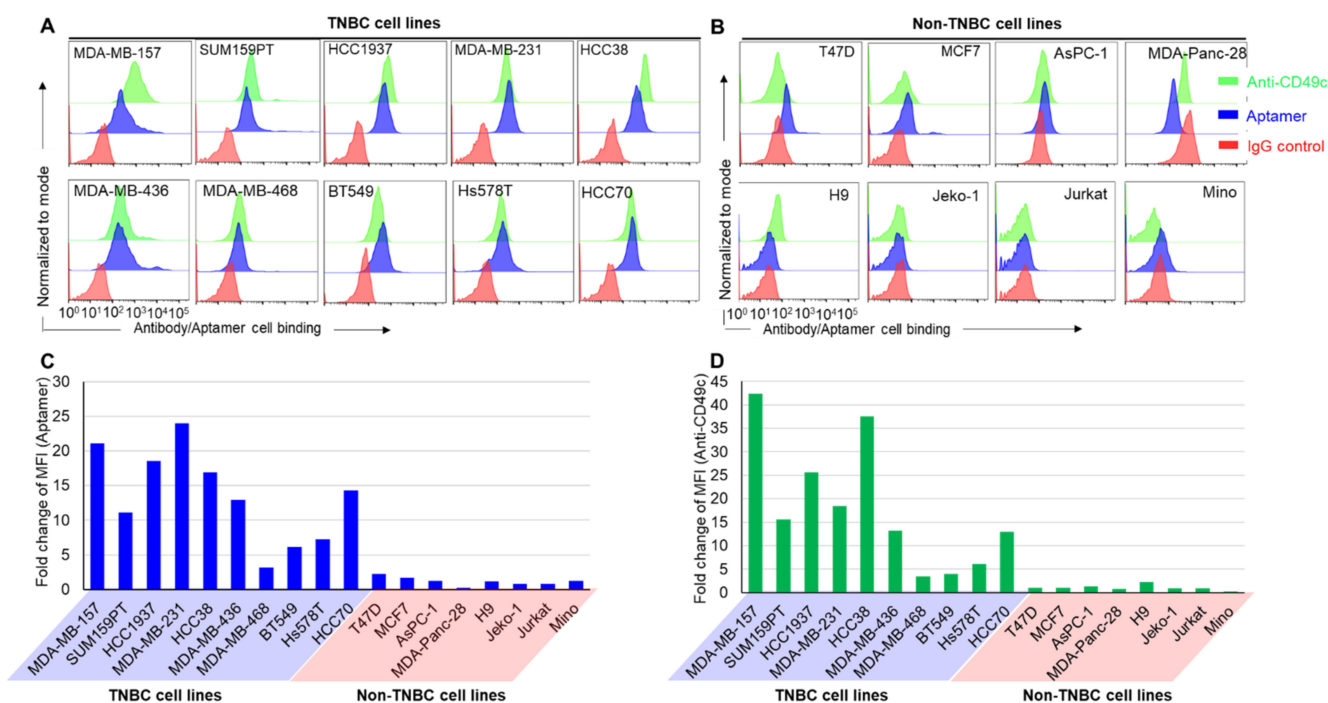


Figure 5. PDGC21T aptamer selectively targets CD49c-expressing TNBC cells. (A) Both PDGC21T aptamer and anti-CD49c targeted TNBC cells with high binding capacity but had (B) little or no binding to non-TNBC cells. Resultant mean fluorescent intensities of cell binding by aptamer (C) and antibody (D) were quantified by flow cytometry and graphed for comparison. The final incubation concentration of aptamer was 200 nM.

Finally, to determine whether the aptamer and antibody were targeting the same site on CD49c, competition binding assays were performed. To evaluate whether anti-CD49c competes with PDGC21T aptamer for cell binding, TNBC cells were pre-incubated with anti-CD49c or IgG isotype control and treated with FAM-labeled PDGC21T aptamer. Flow cytometry analysis showed that PDGC21T aptamer binding to MDA-MB-231 (Figure 6A) and HCC38 cells (Figure 6B) was not affected by pre-incubation with anti-CD49c. In contrast, when TNBC cells were pre-incubated with PDGC21T aptamer, PE-labeled anti-CD49c binding to MDA-MB-231 (Figure 6C) and HCC38 cells (Figure 6D) was significantly reduced, indicating that the binding of PDGC21T aptamers to cells impedes the interaction of the anti-CD49c antibody with cell-surface CD49c, indicating that the PDGC21T aptamer targets CD49c.

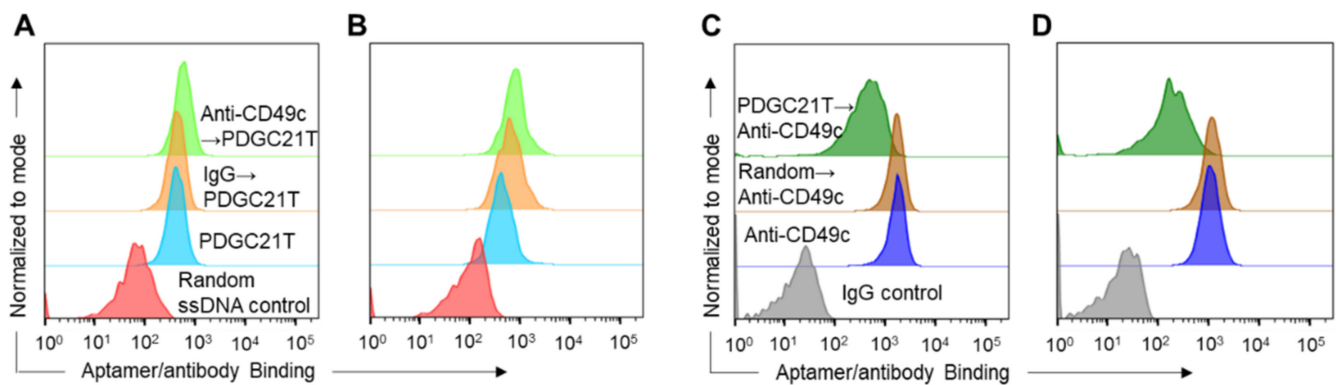


Figure 6. PDGC21T aptamer and anti-CD49c share an overlapping binding site on CD49c. Pre-treatment with anti-CD49c did not affect FAM-labeled PDGC21T aptamer binding to MDA-MB-231 (A) or HCC38 cells (B). IgG isotype and a random ssDNA were used as controls. Pre-treatment with PDGC21T aptamer inhibited PE-labeled anti-CD49c binding to MDA-MB-231 (C) and HCC38 cells (D). Arrows indicate incubation sequence of antibodies and aptamers.

To further confirm that the targeting of PDGC21T to TNBC cell-xenograft tumors was associated with the expression of CD49c, these xenograft tumors were collected and dissociated into single-cell suspensions, followed by being incubated with the Cy3-labeled PDGC21T or the PE-labeled anti-CD49c antibody (Figure S5A). The binding of the aptamer or the antibody was measured using flow cytometry. The results reveal that both the PDGC21T and the anti-CD49c antibody could bind to MDA-MB-231 xenograft-tumor cells (Figure S5B) but not MCF7 xenograft-tumor cells (Figure S5C), suggesting that the PDGC21T aptamer can target those TNBC-xenograft tumor cells with high expression of CD49c.

4. Discussion

Targeted anti-tumor agent delivery is a promising precision therapy for cancer treatment, as it allows the accumulation of anti-tumor agent in tumors via the enhanced permeability and retention effect and active cellular uptake, which reduces adverse side effects while improving therapeutic efficacy [22]. A targeted anti-tumor agent delivery system is principally composed of a targeting ligand that binds a specific surface marker on cancer cells, a spacer and linker, and an optimal anti-tumor agent [23]. Targeting ligands can be nucleic acid aptamers or antibodies. For tumors with known specific cell surface markers, antibodies can serve as excellent targeting ligands [24]. Several clinical trials are investigating antibody-drug conjugates for TNBC therapy [25]. However, for tumors lacking targetable cell surface markers, nucleic acid aptamers may act as ligands for targeted cancer therapy [26]. Indeed, cell-specific aptamers can be readily developed using the cell-SELEX procedure [27].

To detect poorly differentiated gastric cancer cells lacking a targetable molecular marker, Li et al. used the cell-SELEX procedure to develop a 45-nt DNA aptamer (PDGC21T) that selectively targeted poorly differentiated gastric cancer cells [14]. We demonstrated that this aptamer could also target TNBC cell lines in both PBS-based binding buffer and complete DMEM cell culture medium, which suggested that the structure of PDGC21T aptamer was stable in physiological environments. Next, we tested whether the PDGC21T aptamer could target TNBC tumor xenografts in mice. Because PDGC21T binding to MDA-MB-231 cells was stronger relative to other cells (Figure 1), MDA-MB-231 tumor xenografts were used to test the targeting ability of IRDye800CW-labeled PDGC21T [28]. PDGC21T targeted MDA-MB-231 tumor xenografts, but dramatic signal attenuation occurred within 24 h, indicating a short retention time *in vivo*. As unmodified aptamers are susceptible to nuclease-mediated degradation [29], PDGC21T requires chemical modification to extend the circulation time. PEGylation is an eminent aptamer modification used clinically and in

research [21,30]. For therapeutic study, PEGylated PDGC21T aptamer was produced [20], and a validation study revealed that the PEGylated PDGC21T aptamer specifically bound to TNBC cells (MDA-MB-231 and HCC38) and did not react with off-target non-TNBC cells (MCF7). In vivo targeting tests revealed that retention of PEGylated PDGC21T in the liver and spleen exceeded that of non-PEGylated PDGC21T. Furthermore, tumors accumulated more PEGylated PDGC21T and retained the modified aptamers for longer durations relative to non-PEGylated PDGC21T. Further in vivo and ex vivo targeting tests revealed that PEGylated PDGC21T targeted and remained in TNBC xenograft tumors more efficiently than in non-TNBC xenograft tumors. Together, these findings indicate that PEGylated PDGC21T is a promising targeting ligand to facilitate the delivery of anti-TNBC tumor agents.

In addition to their roles as targeting ligands, aptamers are effective agents for cancer biomarker discovery [31,32]. We found that CD49c was the exclusive molecular target of PDGC21T. Cell-binding assays confirmed that PDGC21T exhibited cell-binding patterns mirroring those obtained with a CD49c-specific antibody. A competition assay revealed that while PDGC21T hindered anti-CD49c binding, anti-CD49c did not affect PDGC21T binding, indicating that the PDGC21T-binding region on CD49c overlaps with the antibody-binding region of CD49c. These data verified that CD49c is the target of PDGC21T. CD49c was previously identified as a highly expressed cell surface protein in some TNBC cell lines, including MDA-MB-231, MDA-MB-436, MDA-MB-157, HCC1143, HCC1937, and SUM149PT [33,34]. Furthermore, *ITAG3*, which encodes CD49c, was characterized as a highly expressed gene in pancreatic cancer patients [35]. We found that CD49c was expressed to a lesser degree on the surface of AsPC-1 and MDA-Panc-28 pancreatic adenocarcinoma cell lines (Figure 5B). Although we identified the high expression of CD49c on the surface of TNBC cell lines, CD49c expression in clinical TNBC samples should be further examined.

CD49c is also known as integrin $\alpha 3$ and interacts with integrin $\beta 1$ (CD29) to form the VLA3 integrin receptor that regulates cell adhesion [36,37]. CD49c is considered as a strong contributing factor to tumor invasion. Robust expression levels of VLA3 are related to highly migratory and invasive phenotypes in melanoma [38], head and neck cancer [39], pancreatic cancer [40], intrahepatic cholangiocarcinoma [41], TNBC [42], glioma stem-like cells [43], skin tumor formation, and TNBC and oral squamous cell carcinoma metastases [42,44,45]. Clinical analysis revealed that abundant CD49c was associated with poor prognosis in patients with non-small cell lung cancer [46]. CD49c was also identified as a biomarker of cells undergoing an epithelial-mesenchymal transition in breast cancer [47,48]. Because CD49c promotes tumor progression, reducing CD49c levels using targeted siRNA delivery or blocking CD49c using antibodies or aptamers is a feasible approach to prevent cancer metastasis and progression. In a preclinical study, a monoclonal antibody against aberrantly glycosylated integrin $\alpha 3\beta 1$ was used to block integrin signaling transduction, leading to bladder cancer cell-cycle arrest [49]. Another study used the antibody against activated laminin, the ligand of integrin $\alpha 3\beta 1$, to block the activation of integrin $\alpha 3\beta 1$ signaling to prevent dormant cancer cell awakening [50]. The study suggested that CD49c blockade may help to prevent breast cancer cell awakening.

During PDGC21T target identification in this study, we found that PDGC21T hinders antibody binding to CD49c, but antibody pre-treatment did not influence the binding of PDGC21T aptamer to CD49c. These findings suggest two possible interaction mechanisms of aptamer and antibody to bind CD49c. One possibility is that the aptamer may have multiple binding sites on CD49c protein and one of the sites is shared with the CD49c antibody. Another possibility is that because integrins are well known as conformation changing molecules when interacting with their ligands [51–53], the aptamer binding may trigger a change in the conformation of CD49c protein and thus may have an adverse impact on antibody binding. To testify the first model, CD49c proteins should be gradually truncated to test the binding ability to the PDGC21T aptamer, whereas to verify the second model, X-ray crystal structure of the CD49c-PDGC21T complex should be resolved [54].

The results of the competition assay implies that PDGC21T may inhibit CD49c and laminin interactions to control cancer cell growth, which will be further investigated.

Because CD49c is internalized after binding, it is a promising target for anti-tumor agent delivery [55,56]. Targeting CD49c for chemotherapy and gene therapy has two benefits for cancer control: blocking CD49c to prevent cancer cell metastasis and growth and delivering anti-tumor agents to induce cancer cell death.

5. Conclusions

Here, we identify a TNBC-bound aptamer that may act as a targeting ligand. Furthermore, we identified CD49c as a potential target for antibody or aptamer-guided therapy. Future in vitro and in vivo studies evaluating the therapeutic efficacy of PDGC21T-guided and CD49c-targeted therapies are warranted.

Supplementary Materials: The following supporting information can be downloaded at: <https://www.mdpi.com/article/10.3390/cancers14061570/s1>, Supplemental Material and Methods, Figure S1: PEGylation process for PDGC21T aptamer, Figure S2: Uncropped SDS-PAGE electrophoresis image from Figure S1F, Figure S3: The PEGylated PDGC21T aptamer targeted and remained within HCC1937, HCC38, SUM159PT, and Hs578T xenograft tumors, Figure S4: Uncropped silver-staining images from Figure 4B, Figure S5: Ex vivo binding test of the PDGC21T aptamer and anti-CD49c to xenograft-tumor cells. Table S1: Identification of differential proteins between the PDGC21T aptamer and random ssDNA co-precipitates using LC-MS/MS analysis, Table S2: Quantification analysis for the differential proteins, Table S3: Figure 5-related median fluorescence intensity data. References [16–19] are cited in the Supplementary Materials.

Author Contributions: Conceptualization, Y.Z. (Youli Zu) and Q.W.; methodology, Q.W., Z.Z., J.Q. and Y.Z. (Yingxin Zhao); validation, Y.Z. (Youli Zu) and Q.W.; formal analysis, Q.W.; investigation, Q.W., Z.Z., J.Q. and Y.Z. (Yingxin Zhao); resources, X.L., Z.C. and H.Z.; data curation, Y.Z. (Youli Zu) and Q.W.; writing—original draft preparation, Q.W.; writing—review and editing, Y.Z. (Youli Zu); supervision, Y.Z. (Youli Zu); project administration, Y.Z. (Youli Zu); funding acquisition, Y.Z. (Youli Zu). All authors have read and agreed to the published version of the manuscript.

Funding: The work was partially supported by National Cancer Institute (NCI), grant number R01CA224304.

Institutional Review Board Statement: All procedures were approved by the Institutional Animal Care and Use Committee at Houston Methodist Research Institute (IACUC ID: AUP-1120-0058/IS00006082) and followed the Guidelines from the National Institutes of Health on the Care and Use of Laboratory Animals.

Informed Consent Statement: Not applicable.

Data Availability Statement: Data are contained within this article and in the Supplementary Materials.

Acknowledgments: The authors wish to thank Heather McConnell and Sasha Pejerrey for their scientific editing of the manuscript and Jenny C. Chang at Houston Methodist Academic Institute for the TNBC cell lines.

Conflicts of Interest: The authors declare no conflict of interest.

References

1. Sung, H.; Ferlay, J.; Siegel, R.L.; Laversanne, M.; Soerjomataram, I.; Jemal, A.; Bray, F. Global cancer statistics 2020: GLOBOCAN estimates of incidence and mortality worldwide for 36 cancers in 185 countries. *CA Cancer J. Clin.* **2021**, *71*, 209–249. [[CrossRef](#)] [[PubMed](#)]
2. Waks, A.G.; Winer, E.P. Breast cancer treatment: A Review. *JAMA* **2019**, *321*, 288–300. [[CrossRef](#)] [[PubMed](#)]
3. Foulkes, W.D.; Smith, I.E.; Reis-Filho, J.S. Triple-negative breast cancer. *N. Engl. J. Med.* **2010**, *363*, 1938–1948. [[CrossRef](#)] [[PubMed](#)]
4. Zhong, Y.; Zhao, J.; Li, J.; Liao, X.; Chen, F. Advances of aptamers screened by Cell-SELEX in selection procedure, cancer diagnostics and therapeutics. *Anal. Biochem.* **2020**, *598*, 113620. [[CrossRef](#)]
5. Pang, X.; Cui, C.; Wan, S.; Jiang, Y.; Zhang, L.; Xia, L.; Li, L.; Li, X.; Tan, W. Bioapplications of Cell-SELEX-generated aptamers in cancer diagnostics, therapeutics, theranostics and biomarker discovery: A comprehensive review. *Cancers* **2018**, *10*, 47. [[CrossRef](#)]

6. Chen, M.; Yu, Y.; Jiang, F.; Zhou, J.; Li, Y.; Liang, C.; Dang, L.; Lu, A.; Zhang, G. Development of Cell-SELEX technology and its application in cancer diagnosis and therapy. *Int. J. Mol. Sci.* **2016**, *17*, 2079. [[CrossRef](#)]
7. Shi, H.; Tang, Z.; Kim, Y.; Nie, H.; Huang, Y.F.; He, X.; Deng, K.; Wang, K.; Tan, W. In vivo fluorescence imaging of tumors using molecular aptamers generated by cell-SELEX. *Chem. Asian J.* **2010**, *5*, 2209–2213. [[CrossRef](#)]
8. Yuan, B.; Jiang, X.; Chen, Y.; Guo, Q.; Wang, K.; Meng, X.; Huang, Z.; Wen, X. Metastatic cancer cell and tissue-specific fluorescence imaging using a new DNA aptamer developed by Cell-SELEX. *Talanta* **2017**, *170*, 56–62. [[CrossRef](#)]
9. Shi, H.; Cui, W.; He, X.; Guo, Q.; Wang, K.; Ye, X.; Tang, J. Whole cell-SELEX aptamers for highly specific fluorescence molecular imaging of carcinomas in vivo. *PLoS ONE* **2013**, *8*, e70476. [[CrossRef](#)]
10. Zhou, J.; Rossi, J.J. Cell-specific aptamer-mediated targeted drug delivery. *Oligonucleotides* **2011**, *21*, 1–10. [[CrossRef](#)]
11. Zueva, E.; Rubio, L.I.; Duconge, F.; Tavitian, B. Metastasis-focused cell-based SELEX generates aptamers inhibiting cell migration and invasion. *Int. J. Cancer* **2011**, *128*, 797–804. [[CrossRef](#)]
12. Wu, Y.-Y.; Hsieh, I.S.; Tung, C.-H.; Weng, C.-H.; Wu, J.-E.; Yu, J.-S.; Hong, T.-M.; Chen, Y.-L. A novel DNA aptamer targeting lung cancer stem cells exerts a therapeutic effect by binding and neutralizing Annexin A2. *Mol. Ther. Nucleic Acids* **2022**, *27*, 956–968. [[CrossRef](#)]
13. Berezovski, M.V.; Lechmann, M.; Musheev, M.U.; Mak, T.W.; Krylov, S.N. Aptamer-facilitated biomarker discovery (AptaBiD). *J. Am. Chem. Soc.* **2008**, *130*, 9137–9143. [[CrossRef](#)]
14. Li, W.; Wang, S.; Zhou, L.; Cheng, Y.; Fang, J. An ssDNA aptamer selected by Cell-SELEX for the targeted imaging of poorly differentiated gastric cancer tissue. *Talanta* **2019**, *199*, 634–642. [[CrossRef](#)]
15. Wu, X.; Liu, H.; Han, D.; Peng, B.; Zhang, H.; Zhang, L.; Li, J.; Liu, J.; Cui, C.; Fang, S.; et al. Elucidation and structural modeling of CD71 as a molecular target for cell-specific aptamer binding. *J. Am. Chem. Soc.* **2019**, *141*, 10760–10769. [[CrossRef](#)]
16. Zhang, Y.; Sun, H.; Zhang, J.; Brasier, A.R.; Zhao, Y. Quantitative Assessment of the Effects of Trypsin Digestion Methods on Affinity Purification–Mass Spectrometry-based Protein–Protein Interaction Analysis. *J. Proteome Res.* **2017**, *16*, 3068–3082. [[CrossRef](#)]
17. Cox, J.; Mann, M. MaxQuant enables high peptide identification rates, individualized p.p.b.-range mass accuracies and proteome-wide protein quantification. *Nat. Biotechnol.* **2008**, *26*, 1367–1372. [[CrossRef](#)]
18. Cox, J.; Hein, M.Y.; Lubner, C.A.; Paron, I.; Nagaraj, N.; Mann, M. Accurate proteome-wide label-free quantification by delayed normalization and maximal peptide ratio extraction, termed MaxLFQ. *Mol. Cell. Proteom.* **2014**, *13*, 2513–2526. [[CrossRef](#)]
19. Tusher, V.G.; Tibshirani, R.; Chu, G. Significance analysis of microarrays applied to the ionizing radiation response. *Proc. Natl. Acad. Sci. USA* **2001**, *98*, 5116–5121. [[CrossRef](#)]
20. Prodeus, A.; Abdul-Wahid, A.; Fischer, N.W.; Huang, E.H.; Cydzik, M.; Garipey, J. Targeting the PD-1/PD-L1 immune evasion axis with DNA aptamers as a novel therapeutic strategy for the treatment of disseminated cancers. *Mol. Ther. Nucleic Acids* **2015**, *4*, e237. [[CrossRef](#)]
21. Lu, X.; Zhang, K. PEGylation of therapeutic oligonucleotides: From linear to highly branched PEG architectures. *Nano Res.* **2018**, *11*, 5519–5534. [[CrossRef](#)] [[PubMed](#)]
22. Senapati, S.; Mahanta, A.K.; Kumar, S.; Maiti, P. Controlled drug delivery vehicles for cancer treatment and their performance. *Signal Transduct. Target. Ther.* **2018**, *3*, 7. [[CrossRef](#)]
23. Srinivasarao, M.; Low, P.S. Ligand-targeted drug delivery. *Chem. Rev.* **2017**, *117*, 12133–12164. [[CrossRef](#)] [[PubMed](#)]
24. Parakh, S.; Parslow, A.C.; Gan, H.K.; Scott, A.M. Antibody-mediated delivery of therapeutics for cancer therapy. *Expert Opin. Drug Deliv.* **2016**, *13*, 401–419. [[CrossRef](#)] [[PubMed](#)]
25. Nagayama, A.; Vidula, N.; Ellisen, L.; Bardia, A. Novel antibody-drug conjugates for triple negative breast cancer. *Ther. Adv. Med. Oncol.* **2020**, *12*, 1758835920915980. [[CrossRef](#)] [[PubMed](#)]
26. Sun, H.; Zhu, X.; Lu, P.Y.; Rosato, R.R.; Tan, W.; Zu, Y. Oligonucleotide aptamers: New tools for targeted cancer therapy. *Mol. Ther. Nucleic Acids* **2014**, *3*, e182. [[CrossRef](#)] [[PubMed](#)]
27. Sefah, K.; Shangguan, D.; Xiong, X.; O'Donoghue, M.B.; Tan, W. Development of DNA aptamers using cell-SELEX. *Nat. Protoc.* **2010**, *5*, 1169–1185. [[CrossRef](#)]
28. Cohen, R.; Stammes, M.A.; de Roos, I.H.; Stigter-van Walsum, M.; Visser, G.W.; van Dongen, G.A. Inert coupling of IRDye800CW to monoclonal antibodies for clinical optical imaging of tumor targets. *EJNMMI Res.* **2011**, *1*, 31. [[CrossRef](#)]
29. Zhou, J.; Rossi, J. Aptamers as targeted therapeutics: Current potential and challenges. *Nat. Rev. Drug Discov.* **2017**, *16*, 181–202. [[CrossRef](#)]
30. Ng, E.W.; Shima, D.T.; Calias, P.; Cunningham, E.T., Jr.; Guyer, D.R.; Adamis, A.P. Pegaptanib, a targeted anti-VEGF aptamer for ocular vascular disease. *Nat. Rev. Drug Discov.* **2006**, *5*, 123–132. [[CrossRef](#)]
31. Jin, C.; Qiu, L.; Li, J.; Fu, T.; Zhang, X.; Tan, W. Cancer biomarker discovery using DNA aptamers. *Analyst* **2016**, *141*, 461–466. [[CrossRef](#)]
32. Huang, J.; Chen, X.; Fu, X.; Li, Z.; Huang, Y.; Liang, C. Advances in aptamer-based biomarker discovery. *Front. Cell Dev. Biol.* **2021**, *9*, 659760. [[CrossRef](#)]
33. Yen, T.Y.; Macher, B.A.; McDonald, C.A.; Alleyne-Chin, C.; Timpe, L.C. Glycoprotein profiles of human breast cells demonstrate a clear clustering of normal/benign versus malignant cell lines and basal versus luminal cell lines. *J. Proteome Res.* **2012**, *11*, 656–667. [[CrossRef](#)]

34. Guo, P.; Yang, J.; Liu, D.; Huang, L.; Fell, G.; Huang, J.; Moses, M.A.; Auguste, D.T. Dual complementary liposomes inhibit triple-negative breast tumor progression and metastasis. *Sci. Adv.* **2019**, *5*, eaav5010. [[CrossRef](#)]
35. Jiao, Y.; Li, Y.; Liu, S.; Chen, Q.; Liu, Y. ITGA3 serves as a diagnostic and prognostic biomarker for pancreatic cancer. *OncoTargets Ther.* **2019**, *12*, 4141–4152. [[CrossRef](#)]
36. Bachmann, M.; Kukkurainen, S.; Hytonen, V.P.; Wehrle-Haller, B. Cell adhesion by integrins. *Physiol. Rev.* **2019**, *99*, 1655–1699. [[CrossRef](#)]
37. Michael, M.; Parsons, M. New perspectives on integrin-dependent adhesions. *Curr. Opin. Cell Biol.* **2020**, *63*, 31–37. [[CrossRef](#)]
38. Melchiori, A.; Mortarini, R.; Carlone, S.; Marchisio, P.C.; Anichini, A.; Noonan, D.M.; Albini, A. The $\alpha 3 \beta 1$ integrin is involved in melanoma cell migration and invasion. *Exp. Cell. Res.* **1995**, *219*, 233–242. [[CrossRef](#)]
39. Koshizuka, K.; Hanazawa, T.; Kikkawa, N.; Arai, T.; Okato, A.; Kurozumi, A.; Kato, M.; Katada, K.; Okamoto, Y.; Seki, N. Regulation of ITGA3 by the anti-tumor miR-199 family inhibits cancer cell migration and invasion in head and neck cancer. *Cancer Sci.* **2017**, *108*, 1681–1692. [[CrossRef](#)]
40. Lee, J.; Lee, J.; Choi, C.; Kim, J.H. Blockade of integrin $\alpha 3$ attenuates human pancreatic cancer via inhibition of EGFR signalling. *Sci. Rep.* **2019**, *9*, 2793. [[CrossRef](#)]
41. Huang, Y.; Kong, Y.; Zhang, L.; He, T.; Zhou, X.; Yan, Y.; Zhang, L.; Zhou, D.; Lu, S.; Zhou, J.; et al. High expression of ITGA3 promotes proliferation and cell cycle progression and indicates poor prognosis in intrahepatic cholangiocarcinoma. *Biomed. Res. Int.* **2018**, *2018*, 2352139. [[CrossRef](#)] [[PubMed](#)]
42. Miskin, R.P.; Warren, J.S.A.; Ndoye, A.; Wu, L.; Lamar, J.M.; DiPersio, C.M. Integrin $\alpha 3 \beta 1$ promotes invasive and metastatic properties of breast cancer cells through induction of the Brn-2 transcription factor. *Cancers* **2021**, *13*, 480. [[CrossRef](#)] [[PubMed](#)]
43. Nakada, M.; Nambu, E.; Furuyama, N.; Yoshida, Y.; Takino, T.; Hayashi, Y.; Sato, H.; Sai, Y.; Tsuji, T.; Miyamoto, K.I.; et al. Integrin $\alpha 3$ is overexpressed in glioma stem-like cells and promotes invasion. *Br. J. Cancer* **2013**, *108*, 2516–2524. [[CrossRef](#)] [[PubMed](#)]
44. Sachs, N.; Secades, P.; van Hulst, L.; Kreft, M.; Song, J.Y.; Sonnenberg, A. Loss of integrin $\alpha 3$ prevents skin tumor formation by promoting epidermal turnover and depletion of slow-cycling cells. *Proc. Natl. Acad. Sci. USA* **2012**, *109*, 21468–21473. [[CrossRef](#)] [[PubMed](#)]
45. Nagata, M.; Noman, A.A.; Suzuki, K.; Kurita, H.; Ohnishi, M.; Ohyama, T.; Kitamura, N.; Kobayashi, T.; Uematsu, K.; Takahashi, K.; et al. ITGA3 and ITGB4 expression biomarkers estimate the risks of locoregional and hematogenous dissemination of oral squamous cell carcinoma. *BMC Cancer* **2013**, *13*, 410. [[CrossRef](#)] [[PubMed](#)]
46. Li, Q.; Ma, W.; Chen, S.; Tian, E.C.; Wei, S.; Fan, R.R.; Wang, T.; Zhou, C.; Li, T. High integrin $\alpha 3$ expression is associated with poor prognosis in patients with non-small cell lung cancer. *Transl. Lung Cancer Res.* **2020**, *9*, 1361–1378. [[CrossRef](#)] [[PubMed](#)]
47. Remsik, J.; Fedr, R.; Navratil, J.; Bino, L.; Slabakova, E.; Fabian, P.; Svoboda, M.; Soucek, K. Plasticity and intratumoural heterogeneity of cell surface antigen expression in breast cancer. *Br. J. Cancer* **2018**, *118*, 813–819. [[CrossRef](#)]
48. Shirakihara, T.; Kawasaki, T.; Fukagawa, A.; Semba, K.; Sakai, R.; Miyazono, K.; Miyazawa, K.; Saitoh, M. Identification of integrin $\alpha 3$ as a molecular marker of cells undergoing epithelial-mesenchymal transition and of cancer cells with aggressive phenotypes. *Cancer Sci.* **2013**, *104*, 1189–1197. [[CrossRef](#)]
49. Li, C.; Yang, Z.; Du, Y.; Tang, H.; Chen, J.; Hu, D.; Fan, Z. BCMab1, a monoclonal antibody against aberrantly glycosylated integrin $\alpha 3 \beta 1$, has potent antitumor activity of bladder cancer in vivo. *Clin. Cancer Res.* **2014**, *20*, 4001–4013. [[CrossRef](#)]
50. Albregues, J.; Shields, M.A.; Ng, D.; Park, C.G.; Ambrico, A.; Poindexter, M.E.; Upadhyay, P.; Uyeminami, D.L.; Pommier, A.; Kuttner, V.; et al. Neutrophil extracellular traps produced during inflammation awaken dormant cancer cells in mice. *Science* **2018**, *361*, eaao4227. [[CrossRef](#)]
51. Luo, B.H.; Springer, T.A. Integrin structures and conformational signaling. *Curr. Opin. Cell Biol.* **2006**, *18*, 579–586. [[CrossRef](#)]
52. Askari, J.A.; Buckley, P.A.; Mould, A.P.; Humphries, M.J. Linking integrin conformation to function. *J. Cell Sci.* **2009**, *122*, 165–170. [[CrossRef](#)]
53. Mezu-Ndubuisi, O.J.; Maheshwari, A. The role of integrins in inflammation and angiogenesis. *Pediatr Res.* **2021**, *89*, 1619–1626. [[CrossRef](#)]
54. Khan, N.H.; Bui, A.A.; Xiao, Y.; Sutton, R.B.; Shaw, R.W.; Wylie, B.J.; Latham, M.P. A DNA aptamer reveals an allosteric site for inhibition in metallo-beta-lactamases. *PLoS ONE* **2019**, *14*, e0214440.
55. Das, L.; Anderson, T.A.; Gard, J.M.; Sroka, I.C.; Strautman, S.R.; Nagle, R.B.; Morrissey, C.; Knudsen, B.S.; Cress, A.E. Characterization of laminin binding integrin internalization in prostate cancer cells. *J. Cell. Biochem.* **2017**, *118*, 1038–1049. [[CrossRef](#)]
56. Larrain, J.; Brown, C.; De Robertis, E.M. Integrin- $\alpha 3$ mediates binding of Chordin to the cell surface and promotes its endocytosis. *EMBO Rep.* **2003**, *4*, 813–818. [[CrossRef](#)]